Nanoscale

COMMUNICATION

View Article Online
View Journal

Flexible transparent conducting composite films using a monolithically embedded AgNW electrode with robust performance stability†

Cite this: DOI: 10.1039/c3nr05348b

Received 8th October 2013
Accepted 2nd November 2013

DOI: 10.1039/c3nr05348b

www.rsc.org/nanoscale

Hyeon-Gyun Im,[a] Jungho Jin,[a] Ji-Hoon Ko,[a] Jaemin Lee,[b] Jung-Yong Lee[b] and Byeong-Soo Bae*[a]

We report on the performance of an all-in-one flexible hybrid conducting film employing a monolithically embedded AgNW transparent electrode and a high-performance glass-fabric reinforced composite substrate (AgNW–GFRHybrimer film). Specifically, we perform in-depth investigations on the stability of the AgNW–GFRHybrimer film against heat, thermal oxidation, and wet chemicals to demonstrate the potential of the hybrid conducting film as a robust electrode platform for thin-film optoelectronic devices. With the ease of large-area processability, smooth surface topography, and robust performance stability, the AgNW–GFRHybrimer film can be a promising platform for high-performance optoelectronic devices.

Introduction

Transparent conducting electrodes (TCE) are essential components for modern opto-electric devices such as solar cells, organic light emitting diodes (OLEDs), liquid crystal displays (LCDs), and touch screen panels.[1,2] Indium tin oxide (ITO), the most widely used TCE material to date, has faced challenges mainly due to its limited supply and inherent brittleness, which make it unsuitable for next generation flexible devices.[3] Potential alternatives to ITO include carbon-based TCE such as CNTs, graphene, conducting polymers, and metal nanowires.[2,4–10]

In particular, random networks of silver nanowires (AgNW) are considered the most promising TCE material for the viable replacement of ITO due to their advantages of excellent figure of merit, good flexibility, and compatibility with low-cost solution processes, coupled with their potential for large-size fabrication.[9,10] However, there are still several problems associated with the rough surface topology and weak thermal stability of AgNW TCE that need to be solved for its practical application.[11–13] The surface flatness of AgNW networks should be guaranteed for stable integration of device layers because the intrinsic roughness that stems from NW stacking or percolation causes short circuits that can lead to device failures.

The thermal stability of AgNW-based TCE is another important issue to be addressed because the AgNW networks deposited on a given substrate are usually annealed at an elevated temperature (typically above 200 °C) to achieve better NW–NW contacts, which enable an effective reduction of the sheet resistance.[13–16] However, AgNW-based TCE cannot be fabricated on heat-sensitive substrates such as PET because conventional plastic films are readily deformed when heated to high temperatures.[12,13] In addition, AgNWs are known to melt and coalesce during the thermal annealing process and are likely to be oxidized into thin oxide layers that degrade the electrical performance of TCE.[10] To address these problems, several methods have been reported, such as the embedding of AgNWs in the polymeric matrix and the introduction of additional protective layers on the AgNWs using polymers and graphene.[14,15,17,23] The thermo-mechanical and dimensional stability of flexible TCE films is another set of important requirements in the implementation of reliable device fabrication, because such devices are typically processed at high temperatures and more importantly the TCE is often heated up due to Joule heating.[25] However, conventional plastic films generally do not possess sufficiently reliable thermo-mechanical properties.[12,13,26]

Based on the above considerations, we have previously demonstrated a transparent conducting hybrid plastic film with surface-embedded AgNW TCE (AgNW–GFRHybrimer film); this film can be used as a high-performance flexible TCE platform for organic solar cells.[11] A AgNW–GFRHybrimer film is composed of a glass-fabric reinforced transparent composite (GFRHybrimer) film as a base substrate[18] and spray-deposited AgNW networks as the TCE that are monolithically embedded

[a]Department of Materials Science and Engineering, Korea Advanced Institute of Science and Technology (KAIST), Daejeon, Republic of Korea. E-mail: bsbae@kaist.ac.kr; Fax: +82-42-350-3310; Tel: +82-42-350-4119

[b]Graduate School of Energy, Environment, Water, and Sustainability (EEWS), Korea Advanced Institute of Science and Technology (KAIST), Daejeon, Republic of Korea

† Electronic supplementary information (ESI) available: Further characteristics of AgNW–GFRHybrimer films and thermal oxidation of AgNW on glass. See DOI: 10.1039/c3nr05348b

on the film surface; the term '*monolithically*' is used to illustrate a point that our hybrid conducting film is an all-in-one AgNW TCE/substrate film. The robust monolithic hybrid structure of the AgNW–GFRHybrimer film has enabled unprecedentedly smooth surface topology (<2 nm), good thermo-mechanical performance (CTE ~ 15 ppm $°C^{-1}$ and T_g less characteristics), and an excellent opto-electrical property (R_{sh} ~ 22 Ω sq^{-1} and T = 85%). Herein, we report on detailed investigations into the durability of the AgNW–GFRHybrimer film against heat-treatment, thermal-oxidation, and wet chemical processes, all of which are associated with the process environment for the fabrication of typical thin-film optoelectronic devices.

Results and discussion

AgNW–GFRHybrimer films (R_{sh} ~ 20 Ω sq^{-1} and T = 84%) were fabricated with the method reported in our previous publication[11] (Fig. 1, also see the ESI†). Briefly, AgNW networks spray-deposited on a donor glass were directly transferred onto the matrix resin-impregnated glass-fabric sheet (*i.e.*, prepreg) prepared on a counter glass *via* a vacuum-assisted sheet molding process. The freestanding AgNW–GFRHybrimer film was then separated after UV-curing of the matrix resin. With the aid of the AgNW spray-deposition process, which is suited for large-area fabrication, an AgNW–GFRHybrimer film with a size as large as 10 × 10 cm^2 can be fabricated (Fig. 1b). The monolithic transfer of AgNW networks onto the surface of the base film allows tight encapsulation of the AgNW, resulting in an exceptionally smooth surface topography of the embedded AgNW electrode (Fig. 1c and Fig. S2†).

To evaluate the thermal stability in terms of the electrical performance, the as-prepared AgNW–GFRHybrimer films were oven-annealed under the following temperature/atmospheric conditions for 6 hours: 200 °C/N_2, 200 °C/air, 250 °C/N_2, and 250 °C/air. The corresponding samples are designated as 200N, 200A, 250N, and 250A, respectively. The sheet resistance (R_{sh}) of each sample was measured simultaneously during thermal annealing using a 4-point probe sheet resistance meter every 30 min. For 200A, 200N, and 250N, the R_{sh} values were retained even after the long annealing time (6 hours) without any dimensional changes or deformation of the hybrid film such as warping or curling (Fig. 2a and b). This result confirms that AgNW–GFRHybrimer films are thermally stable up to 200 °C regardless of the atmospheric conditions and even to 250 °C in an inert atmosphere (250N). This long-term high-thermal stability of AgNW–GFRHybrimer films, coupled with the smooth AgNW topography, is a promising feature that affords stable integration of device layers such as metal oxide

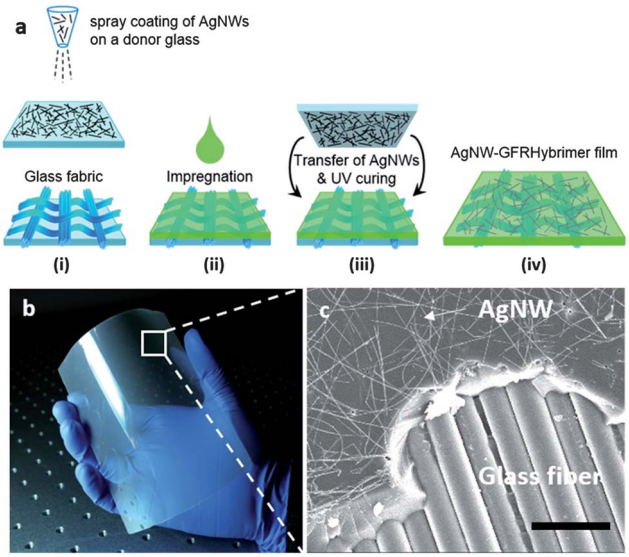

Fig. 1 (a) Fabrication procedure of the AgNW–GFRHybrimer film; (i and ii) AgNW solution is spray-deposited on a donor glass while glass fabrics are placed on another donor glass, followed by impregnating the glass-fabrics with the matrix resin to form a prepreg, (iii) the two glasses are then compressed *via* a vacuum-assisted sheet molding process and subsequently the sample is UV-cured, (iv) a free-standing AgNW–GFRHybrimer film is obtained after separating the glasses. (b) Optical image of a 10 × 10 cm^2 AgNW–GFRHybrimer film (R_{sh} = 20 Ω sq^{-1}, 84% transmittance at 550 nm). A AgNW–GFRHybrimer film is as highly flexible as it can be rolled on a 2.5 mm diameter mandrel without any degradation in the sheet resistance or film deformation (Fig. S1†).[18] (c) Surface SEM image of the AgNW–GFRHybrimer film showing AgNW networks monolithically integrated on the surface of the base composite film. The scale bar is 10 μm.

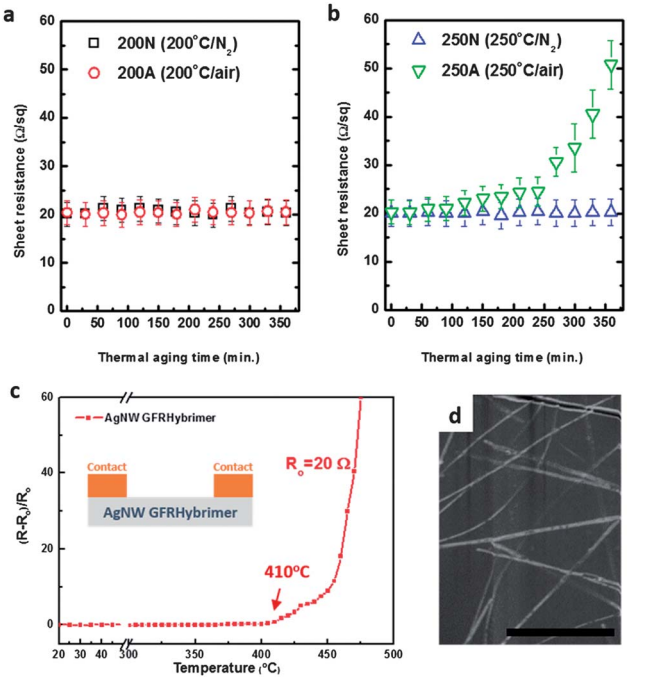

Fig. 2 Thermal stability of the AgNW–GFRHybrimer film. (a and b) Plots of R_{sh} *vs.* annealing time for the AgNW–GFRHybrimer film with varying temperature and atmospheric test conditions (200 °C/N_2; 200N, 200 °C/air; 200A, 250 °C/N_2; 250N, 250 °C/air; 250A, respectively). R_{sh} values were retained after annealing at 200N, 200A, and 250N. For 250A, R_{sh} was increased up to 50 Ω sq^{-1} after annealing for 360 minutes. (c) Plot of the normalized R_{sh} change of the AgNW–GFRHybrimer film with elevating temperatures (the initial sheet resistance R_o = 20 ohm sq^{-1}, ramp rate = 5 °C min^{-1}). Note that the electrical performance was maintained up to 410 °C and then rapidly degraded. (d) SEM image of the surface of the AgNW–GFRHybrimer film after the thermal test (c). The scale bar is 5 μm.

interfacial layers and active organic layers in typical organic thin-film optoelectronic devices;[11,24] such integration is not commonly achievable with normal AgNW-based TCE deposited on conventional plastic films due to their limited higher operating temperatures.[26] The electrical performance of the AgNW–GFRHybrimer was stable even under the 250 °C/air condition (250A) for 2 hours (Fig. 2b). However, prolonged annealing of the 250A sample resulted in an exponential increase of R_{sh}, which was likely due to both the thermal oxidation of AgNW[20] and the decomposition of the matrix. The thermal stability of AgNW–GFRHybrimer films was further confirmed in an additional test (Fig. 2c), in which an AgNW–GFRHybrimer film was annealed up to 500 °C on a hot-plate with a ramp rate of 5 °C min^{-1}; the film's R_{sh} value was checked *in situ* every minute. For this *in situ* tracking of resistance, two separate electrical outlets were directly created on the film using silver paste (see the inset in Fig. 2c). This test may provide technically relevant information for the fabrication of typical thin-film optoelectronic devices employing embedded AgNW electrodes since the integration of the device layers is often carried out on a hot-plate in laboratory-scale research. Upon annealing, the R_{sh} of the AgNW–GFRHybrimer film maintained its initial resistance (20 Ω sq^{-1}) until 410 °C and then surged exponentially. Note that the embedded AgNW networks in the hybrid film are intact without any meltdown or disconnections even after the test (Fig. 2d). This high-temperature durability of the AgNW–GFRHybrimer film stems from the fact that the AgNW network is effectively protected by the thermally stable matrix as expected from the encapsulated AgNW morphology.[14] To clarify the thermal insulation effect conferred by the matrix encapsulation, a standard AgNW TCE formed on glass is also tested under the same conditions as a control (Fig. S3†). As expected, the AgNW TCE on glass ended up with severe meltdown and degradation of the electrical performance at lower temperatures.[10]

Upon high-temperature annealing, most plastic films undergo thermal degradation often resulting in deterioration of their optical transparency. Thus, the change in the optical transparency of a typical TCE film is another relevant standard by which the thermal stability of the TCE system can be assessed. In the following experiments, the optical transmittance values of AgNW–GFRHybrimer films (84% at 550 nm) were traced every 30 min under the same environmental conditions (Fig. 3), which show a consistent trend as in the case of the electrical performance. For 200A, 200N, and 250N, the UV-vis spectra show little variation in the transmittance value over the entire period without any discolorations (photographs shown in the inset of Fig. 3a and b) confirming the excellent thermal stability of AgNW–GFRHybrimer films. Even for the 250A film, the transmittance value did not change until the 30 min mark. However, the 250A film ends up with drastic degradation of the transmittance down to 45% after 6 hours of annealing with a serious yellowing phenomenon; this deterioration is primarily due to the radical-activated oxidative degradation of the organic phases in the matrix material.[21]

The thermal oxidation stability of the AgNW–GFRHybrimer films – 200N, 200A, 250N, and 250A – is investigated by XRD and SEM analyses (Fig. 4). In the XRD pattern (Fig. 4a), the peaks at

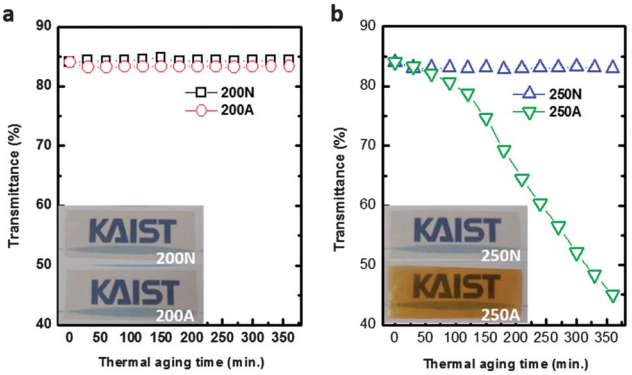

Fig. 3 Optical property of AgNW–GFRHybrimer films according to the thermal aging time. (a) Optical transparency was maintained without discoloration after the annealing process for 360 minutes for both 200N and 200A. (b) Yellowing occurred with the decreasing transmittance while annealing at 250A. In contrast, 250N showed retained transparency. The inset images are AgNW–GFRHybrimer films after the thermal annealing test.

$2\theta = 44°$, $2\theta = 38°$, and $2\theta = 32.4°$ are assigned to Ag (200), Ag (111), and Ag_2O, respectively.[19,20] For 200N, 200A, and 250N, only the characteristic peaks from the metallic Ag phase are shown and no peak from Ag_2O is observed. Correspondingly,

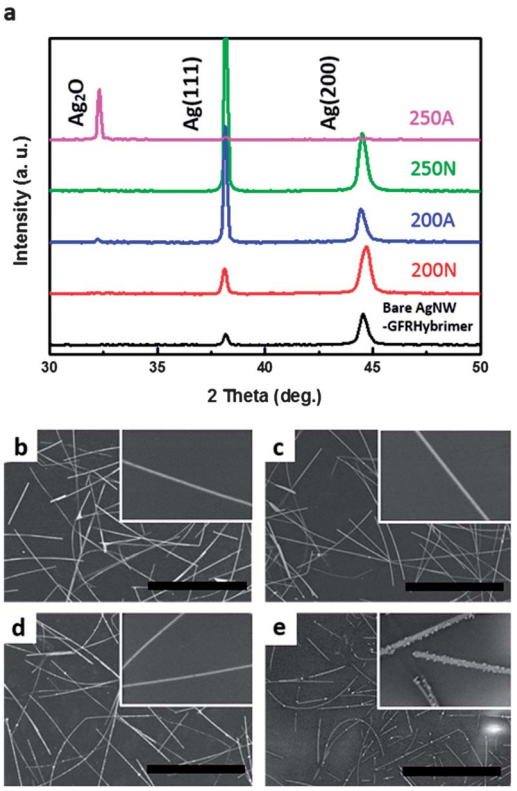

Fig. 4 (a) XRD patterns of AgNW–GFRHybrimer films after annealing under varying conditions. Metallic silver peaks (111) and (200) remained after annealing of 200N, 200A and 250N. (b–e) Surface SEM images of AgNW–GFRHybrimer films (b, c, d and e represent 200N, 200A, 250N and 250A, respectively). Clean surfaces of AgNWs were observed in (b)–(d). (e) Silver oxide particles are shown on the surface of the AgNW. All the scale bars are 20 μm.

the SEM images of 200N, 200A, and 250N show smooth AgNW morphology confirming that there is no signature of thermal oxidation of AgNW.[15] These results illustrate the excellent thermal-oxidation resistance of the AgNW electrode in the AgNW–GFRHybrimer film due to the monolithically embedded structure and are also consistent with the results from the thermal stability test (Fig. 2). However, the oxidation of AgNW is found for the 250A film as evidenced by the appearance of the Ag_2O peak in the XRD pattern. This AgNW oxidation is further confirmed from the SEM image of the 250A film which shows Ag_2O particles decorated on the surface.[15,20] It is noteworthy that the peaks for metallic Ag completely disappear after 6 hours of total annealing (250A, in Fig. 4a). This result indicates that most of the metallic Ag phase is transformed to Ag_2O possibly due to the fact that, at 250 °C, diffusion of O_2 is kinetically activated.[15,20] We further examined the thermal oxidation behavior of the 250A film as a function of the annealing time and found that the phase transformation to Ag_2O occurs after 2 hours (Fig. S4†).

Tolerance against chemical attack is another important issue to be addressed for viable application of an AgNW-based TCE system. This is particularly true in a sense that most of the device fabrication processes involve chemicals that may degrade the bottom AgNW electrode. In general, such chemical attacks are often facilitated in nanostructured AgNW due to its high surface area.[14,19] To determine the chemical stability of the AgNW–GFRHybrimer film, we used 5 wt% of K_2S aqueous solution as an oxidative reagent because silver is known to be sulfurated upon exposure to sulfur-containing compounds.[14,19] The experiment was set up in such a manner that a certain amount of the K_2S solution was spread on the surface of an AgNW–GFRHybrimer film that has two separate electrical outlets made of silver paste. The normalized change in sheet resistance ($R - R_0/R_0$) was then traced *in situ* using a resistance meter (Fig. 5a). A spray-deposited AgNW electrode on glass was used as the control. Upon chemical attack by K_2S solution, the R_{sh} of the control sample surged catastrophically after 50 s due to the sulfuration of the AgNW on the glass substrate; this is also confirmed from the SEM image (Fig. 5b). In contrast, the electrical performance of the AgNW–GFRHybrimer film was fairly stable until 150 s, confirming the superior chemical stability of the AgNW–GFRHybrimer film. The excellent chemical stability of the AgNW–GFRHybrimer film can be attributed to the minimal exposure of the embedded AgNW. However, although no indication of AgNW corrosion was observed in the SEM analysis (Fig. 5c), the R_{sh} of the AgNW–GFRHybrimer film increased exponentially after 150 s. This result may stem from the lack of AgNW–matrix interfacial binding in terms of chemical bonding despite the embedded structure that allows the permeation of the chemical.[14,15]

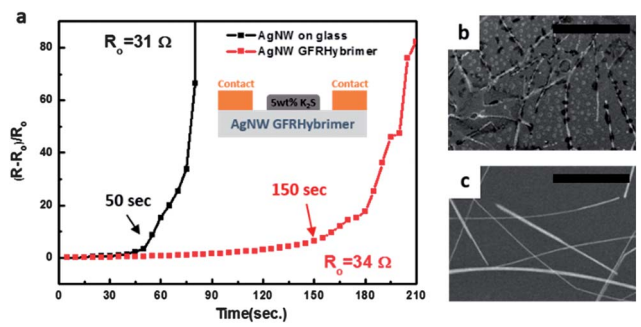

Fig. 5 Chemical stability of the AgNW–GFRHybrimer film (K_2S corrosion test). (a) Plot of the normalized R_{sh} change *vs.* corrosion time (the initial sheet resistance R_0 is 31 Ω sq^{-1}). Surface SEM images of AgNWs on (b) glass (control), and (c) AgNW–GFRHybrimer film. All scale bars represent 5 μm.

Conclusion

In conclusion, we have demonstrated an all-in-one transparent hybrid conducting film using monolithically embedded AgNW and a high-performance fiber reinforced composite film. The AgNW–GFRHybrimer film shows excellent stability against heat, thermal-oxidation, and chemical attack due to the embedded structure of the AgNW electrode with the robust matrix. Electrical and optical performances of the AgNW–GFRHybrimer film were found to be strongly durable even during long-term high-temperature annealing (250 °C, inert atmosphere). The chemical stability of the AgNW–GFRHybrimer was further confirmed by an extended duration time in the K_2S corrosion test. These results may provide further insight into the fabrication of optoelectronic devices employing typical embedded AgNW TCE systems. With the ease of large-area processability, smooth surface topology, and excellent stability, a AgNW–GFRHybrimer film can be a promising platform for high-performance optoelectronic devices.

Experimental

Synthesis and spray-deposition of AgNW

AgNWs were synthesized by a modified recipe reported by Yang *et al.*[22] and then spray-coated on a donor carrier glass. An automated spray-coating machine was used to prepare the AgNW TCE on the donor glass. The back pressure (N_2) was 0.1 MPa and the flow rate of the AgNW solution was 3 ml min^{-1}. The distance between the substrate and the nozzle was fixed to 13 cm for uniform distribution of AgNWs. The substrate temperature was 100 °C for evaporation of the solvent immediately. The scan speed of the nozzle was 4000 inch per min, and the moisture in the spraying booth was maintained at 30%. The concentration of the solution was 0.6 mg ml^{-1}.

Characterization

The sheet resistance of the AgNW–GFRHybrimer film was measured with a 4-point probe sheet resistance meter, and the measured R_{sh} values were also cross-checked using a multimeter as we previously reported.[11] The SEM images of the AgNW–GFRHybrimer film were obtained using a scanning electron microscope (s4800, HITACHI). XRD analysis was conducted using a multi-purpose high power X-ray diffractometer (Rigaku, D/Max-2500) in the scan range of $2\theta = 30$–90 with the scan speed of 2° min^{-1}, the step size of 0.01°, and the power of

40 kV and 300 mA. The optical transparency was obtained in a wavelength range between 350 nm and 800 nm using an ultraviolet-visible-near infrared (UV/vis/NIR) spectrophotometer (Shimadzu, UV3101PC).

Acknowledgements

This work was supported by the National Research Foundation of Korea (NRF) grant funded by the Korea government (MSIP) (CAFDC/Byeong-Soo Bae/no. 2007-0056090).

Notes and references

1 R. G. Gordon, *MRS Bull.*, 2000, **25**, 52–57.
2 Z. C. Wu, Z. H. Chen, X. Du, J. M. Logan, J. Sippel, M. Nikolou, K. Kamaras, J. R. Reynolds, D. B. Tanner, A. F. Hebard and A. G. Rinzler, *Science*, 2004, **305**, 1273–1276.
3 Y. Leterrier, L. Medico, F. Demarco, J. A. E. Manson, U. Betz, M. F. Escol, M. K. Olsson and F. Atamny, *Thin Solid Films*, 2004, **460**, 156–166.
4 L. Hu, D. S. Hecht and G. Gruner, *Chem. Rev.*, 2010, **110**, 5790–5844.
5 V. N. Popov, *Mater. Sci. Eng., R*, 2004, **43**, 61–102.
6 K. Tvingstedt and O. Inganas, *Adv. Mater.*, 2007, **19**, 2893–2897.
7 D. L. Carroll, R. Czerw and S. Webster, *Synth. Met.*, 2005, **155**, 694–697.
8 S. Bae, H. Kim, Y. Lee, X. Xu, J.-S. Park, Y. Zheng, J. Balakrishnan, T. Lei, H. R. Kim, Y. I. Song, Y.-J. Kim, K. S. Kim, B. Özyilmaz, J.-H. Ahn, B. H. Hong and S. Iijima, *Nat. Nanotechnol.*, 2010, **5**, 574–578.
9 Y. Sun, *Nanoscale*, 2010, **2**, 1626–1642.
10 J.-Y. Lee, S. T. Connor, Y. Cui and P. Peumans, *Nano Lett.*, 2008, **8**, 689–692.
11 J. Jin, J. Lee, S. Jeong, S. C. Yang, J.-H. Ko, H.-G. Im, S.-W. Baek, J.-Y. Lee and B.-S. Bae, *Energy Environ. Sci.*, 2013, **6**, 1811–1817.
12 T. Tokuno, M. Nogi, J. Jiu and K. Suganuma, *Nanoscale Res. Lett.*, 2012, **7**, 281.
13 V. Scardaci, R. Coull, P. E. Lyons, D. Rickard and J. N. Coleman, *Small*, 2011, **7**, 2621–2628.
14 X. Y. Zeng, Q. K. Zhang, R. M. Yu and C. Z. Lu, *Adv. Mater.*, 2010, **22**, 4484–4488.
15 Y. Ahn, Y. Jeong and Y. Lee, *ACS Appl. Mater. Interfaces*, 2012, **4**, 6410–6414.
16 J. Lee, I. Lee, T. S. Kim and J. Y. Lee, *Small*, 2013, **9**, 2887–2894.
17 W. Gaynor, G. F. Burkhard, M. D. McGehee and P. Peumans, *Adv. Mater.*, 2011, **23**, 2905–2910.
18 J. Jin, J. H. Ko, S. C. Yang and B. S. Bae, *Adv. Mater.*, 2010, **22**, 4510.
19 J. L. Elechiguerra, L. Larios-Lopez, C. Liu, D. Garcia-Gutierrez, A. Camacho-Bragado and M. Yacaman, *J. Chem. Eng. Mater. Sci.*, 2005, **17**, 6042–6052.
20 G. I. N. Waterhouse, G. A. Bowmaker and J. B. Metson, *Phys. Chem. Chem. Phys.*, 2001, **3**, 3838–3845.
21 S. Yang, S. Y. Kwak, J. Jin, J. S. Kim, Y. Choi, K. W. Paik and B. S. Bae, *J. Mater. Chem.*, 2012, **22**, 8874.
22 C. Yang, H. W. Gu, W. Lin, M. M. Yuen, C. P. Wong, M. Y. Xiong and B. Gao, *Adv. Mater.*, 2011, **23**, 3052–3056.
23 M. S. Lee, K. Lee, S. Y. Kim, H. Lee, J. Park, K. H. Choi, H. K. Kim, D. G. Kim, D. Y. Lee, S. W. Nam and J. U. Park, *Nano Lett.*, 2013, **13**, 2814–2821.
24 D. S. Leem, A. Edwards, M. Faist, J. Nelson, D. D. C. Bradley and J. C. de Mello, *Adv. Mater.*, 2011, **23**, 4371–4375.
25 H. H. Khaligh and I. A. Goldthorpe, *Nanoscale Res. Lett.*, 2013, **8**, 235.
26 M. C. Choi, Y. Kim and C. S. Ha, *Prog. Polym. Sci.*, 2008, **33**, 581–630.